



# Measurement of the CKM angle $\gamma$ using $B_s^0 \rightarrow D_s K \pi \pi$ decays

P. d'Argent<sup>1</sup>, E. Gersabeck<sup>1</sup>, M. Kecke<sup>1</sup>, M. Schiller<sup>2</sup>

<sup>1</sup>*Physikalisches Institut, Ruprecht-Karls-Universität Heidelberg, Heidelberg, Germany*

<sup>2</sup>*School of Physics and Astronomy, University of Glasgow, Glasgow, United Kingdom*

## Abstract

We present the first measurement of the weak phase  $2\beta + \gamma$  obtained from a time-dependent (amplitude) analysis of  $B_s^0 \rightarrow D_s K \pi \pi$  decays using proton-proton collision data corresponding to an integrated luminosity of **xxx** fb<sup>-1</sup> recorded by the LHCb detector.



# Contents

<b>0</b>	<b>To Do List with Assignment of Tasks</b>	<b>1</b>
<b>1</b>	<b>Introduction</b>	<b>2</b>
<b>2</b>	<b>Sensitivity studies</b>	<b>3</b>
2.1	PDF . . . . .	3
2.2	Estimation of coherence factor . . . . .	4
2.3	Results . . . . .	6
<b>3</b>	<b>Selection</b>	<b>9</b>
3.1	Cut-based selection . . . . .	9
3.2	Multivariate stage . . . . .	11
<b>4</b>	<b>Decay-time Acceptance</b>	<b>15</b>
<b>5</b>	<b>Decay-time Resoution</b>	<b>18</b>
5.1	Formalism . . . . .	18
5.2	Results . . . . .	18
	<b>References</b>	<b>20</b>

## 0 To Do List with Assignment of Tasks

### 1. MC Requests (Urgent !):

Run-2 MC

Phasespace MC for Dalitz Eff

(need much higher statistics, filtered request ? on what ?)

Ds  $\rightarrow$  3pi MC ?

Part. reco. bkg MC ?

With CPV ?

### 2. Selection:

Reoptimize with phasespace cuts (e.g.  $m(KK\pi) < 2GeV$  ) ?

### 3. Use Meerkat PID resampling

(<https://twiki.cern.ch/twiki/bin/view/LHCb/MeerkatPIDResampling>)

### 4. Tagging:

Produce new samples with tagging info (Matthieu, Philippe)

Calibration

### 5. Acceptance: (Matthieu)

Compare data and MC

### 6. Resolution: (Matthieu)

Compare  $Bs \rightarrow DsK$  and  $Bs \rightarrow DsK\pi\pi$  MC

Get LTU  $Bs \rightarrow DsK$  data sample ?

### 7. TD-MINT: (Philippe)

Resolution integrals

per-event tagging

# 1 Introduction

The weak phase  $\gamma$  is the least well known angle of the CKM unitary triangle. A key channel to measure  $\gamma$  is the time-dependent analysis of  $B_s^0 \rightarrow D_s K$  decays [1], [2]. The  $B_s^0 \rightarrow D_s K \pi \pi$  proceeds at tree level via the transitions shown in Fig. 1.1 a) and b).

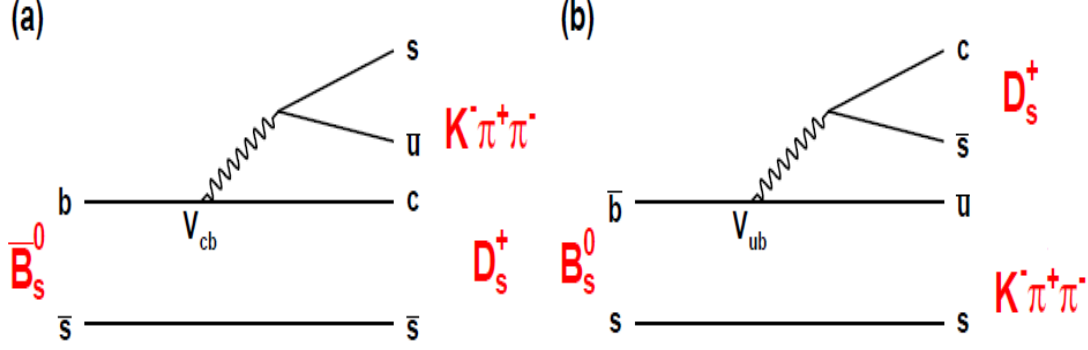


Figure 1.1: Feynman diagram of the  $B_s^0 \rightarrow D_s K \pi \pi$  decay, proceeding via a)  $b \rightarrow c$  transitions or b)  $b \rightarrow u$  transitions.

To measure the weak CKM phase  $\gamma \equiv \arg[-(V_{ud}V_{ub}^*)/(V_{cd}V_{cb}^*)]$ , a decay with interference between  $b \rightarrow c$  and  $b \rightarrow u$  transitions at tree level is needed [1]. As illustrated in Fig. 1.1, this is the case for the presented decay mode. A measurement of  $\gamma$  using  $B_s^0 \rightarrow D_s K \pi \pi$  decays, where the  $K \pi \pi$  subsystem is dominated by excited kaon states such as the  $K_1(1270)$  and  $K_1(1400)$  resonances, will succeed the branching ratio measurement presented in this note. It is complementary to the above mentioned analysis of  $B_s^0 \rightarrow D_s K$ , making use of a fully charged final state, where every track is detected in the vertex locator. To account for the non-constant strong phase across the Dalitz plot, one can either develop a time-dependent amplitude model or select a suitable phase-space region and introduce a coherence factor as additional hadronic parameter to the fit. This analysis is based on the first observation of the  $B_s^0 \rightarrow D_s K \pi \pi$  decay presented in [3] and [4], where its branching ratio is measured relative to  $B_s^0 \rightarrow D_s \pi \pi \pi$ . The result obtained by the previous analysis is  $0.052 \pm 0.005 \pm 0.003$ , where the uncertainties are statistical and systematical, respectively. The branching ratio measurement is updated, exploiting the full Run 1 data sample, corresponding to  $3 \text{ fb}^{-1}$  of integrated luminosity.

## 2 Sensitivity studies

### 2.1 PDF

First, I define the purely hadronic amplitudes for a given phasespace point  $x$ . The weak phase dependence is written latter explicitly in the pdf.

$$A(B_s^0 \rightarrow D_s^- K^+ \pi \pi) \equiv A(x) = \sum_i a_i A_i(x) \quad (2.1)$$

$$A(B_s^0 \rightarrow D_s^+ K^- \pi \pi) \equiv \bar{A}(\bar{x}) = \sum_i \bar{a}_i \bar{A}_i(\bar{x}) \quad (2.2)$$

$$A(\bar{B}_s^0 \rightarrow D_s^- K^+ \pi \pi) = \bar{A}(x) \text{ (Assuming no direct CPV)} \quad (2.3)$$

$$A(\bar{B}_s^0 \rightarrow D_s^+ K^- \pi \pi) = A(\bar{x}) \text{ (Assuming no direct CPV)} \quad (2.4)$$

The full time-dependent amplitude pdf is given by:

$$\begin{aligned} P(x, t, q_t, q_f) \propto & [ (|A(x)|^2 + |\bar{A}(x)|^2) \cosh\left(\frac{\Delta\Gamma t}{2}\right) \\ & + q_t q_f (|A(x)|^2 - |\bar{A}(x)|^2) \cos(m_s t) \\ & - 2\text{Re}(A(x)^* \bar{A}(x) e^{-iq_f(\gamma-2\beta_s)}) \sinh\left(\frac{\Delta\Gamma t}{2}\right) \\ & - 2q_t q_f \text{Im}(A(x)^* \bar{A}(x) e^{-iq_f(\gamma-2\beta_s)}) \sin(m_s t) ] e^{-\Gamma t} \end{aligned}$$

where  $q_t = +1$  ( $-1$ ) for a  $B_s^0$  ( $\bar{B}_s^0$ ) tag and  $q_f = +1$  ( $-1$ ) for  $D_s^- K^+ \pi \pi$  ( $D_s^+ K^- \pi \pi$ ) final states.

Integrating over the phasespace, we get

$$\begin{aligned} \int P(x, t, q_t, q_f) dx \propto & [ \cosh\left(\frac{\Delta\Gamma t}{2}\right) \\ & + q_t q_f \left(\frac{1-r^2}{1+r^2}\right) \cos(m_s t) \\ & - 2 \left(\frac{\kappa r \cos(\delta - q_f(\gamma - 2\beta_s))}{1+r^2}\right) \sinh\left(\frac{\Delta\Gamma t}{2}\right) \\ & - 2q_t q_f \left(\frac{\kappa r \sin(\delta - q_f(\gamma - 2\beta_s))}{1+r^2}\right) \sin(m_s t) ] e^{-\Gamma t} \\ = & [ \cosh\left(\frac{\Delta\Gamma t}{2}\right) + q_t q_f C \cos(m_s t) - \kappa D_{q_f} \sinh\left(\frac{\Delta\Gamma t}{2}\right) - q_t \kappa S_{q_f} \sin(m_s t) ] e^{-\Gamma t} \end{aligned}$$

where the  $C, D_{q_f}, S_{q_f}$  are defined exactly as for  $D_s K$ . The coherence factor is defined as :

$$\kappa e^{i\delta} \equiv \frac{\int A(x)^* \bar{A}(x) dx}{\sqrt{\int |A(x)|^2 dx} \sqrt{\int |\bar{A}(x)|^2 dx}} \quad (2.5)$$

$$r \equiv \frac{\sqrt{\int |\bar{A}(x)|^2 dx}}{\sqrt{\int |A(x)|^2 dx}} \quad (2.6)$$

and appears in front of the  $D_{q_f}, S_{q_f}$  terms. This means one additional fit parameter for the lifetime fit. In the limit of only one contributing resonance  $\kappa \rightarrow 1$ .

## 2.2 Estimation of coherence factor

To estimate the coherence factor we could generate many toys with random  $a_i$  and  $\bar{a}_i$  values (see [https://twiki.cern.ch/twiki/pub/LHCbPhysics/Bu2DKstar/LHCb-ANA-2017-005\\_v1.pdf](https://twiki.cern.ch/twiki/pub/LHCbPhysics/Bu2DKstar/LHCb-ANA-2017-005_v1.pdf)) using the set of amplitudes show in our last talk. However with so many interfering amplitudes, I would be surprised if you couldn't generate every possible value for  $\kappa$ . In any case, this would give us a range where to expect possible values for  $\kappa$ . Worst case would be  $0 \leq \kappa \leq 1$ .

Assumptions:

- $A(x) = \sum_i a_i A_i(x)$   
 $\bar{A}(x) = \sum_i \bar{a}_i \bar{A}_i(x)$
- Use amplitudes from flavor-averaged, time-integrated fit
- Draw random  $a_i$  and  $\bar{a}_i$  values
- Constraints:  
 $\int (|a_i A_i(x)|^2 + |\bar{a}_i \bar{A}_i(x)|^2) dx / N = F_i^{eff}$   
 $r \approx 0.4$  (ration of CKM elements)

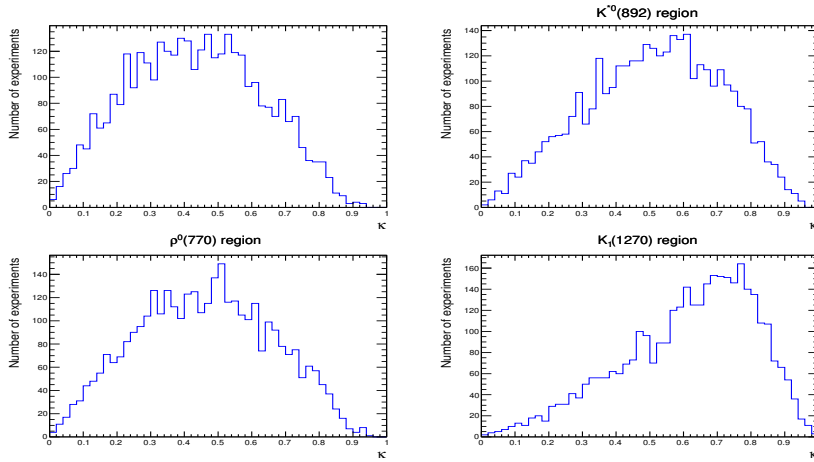


Figure 2.1

Table 2.1

Region	$< \kappa > (\%)$	Cut eff. (%)
Full	43	100
$K^*(892)$	51	43
$\rho^0(770)$	46	47
$K_1(1270)$	61	23



## 2.3 Results

Assumptions:

- Use amplitudes from flavor-averaged, time-integrated fit
- $r = 0.4$  (ratio of CKM elements)
- PDG values for:  $\tau, \Delta m_s, \Delta \Gamma, \beta_s$
- $\epsilon(x, t) = \text{const.}$ , perfect resolution
- $\epsilon_{Tag} = 0.66, < \omega > = 0.4$
- $N_{signal} = 3000$  (Run1+15/16 data)

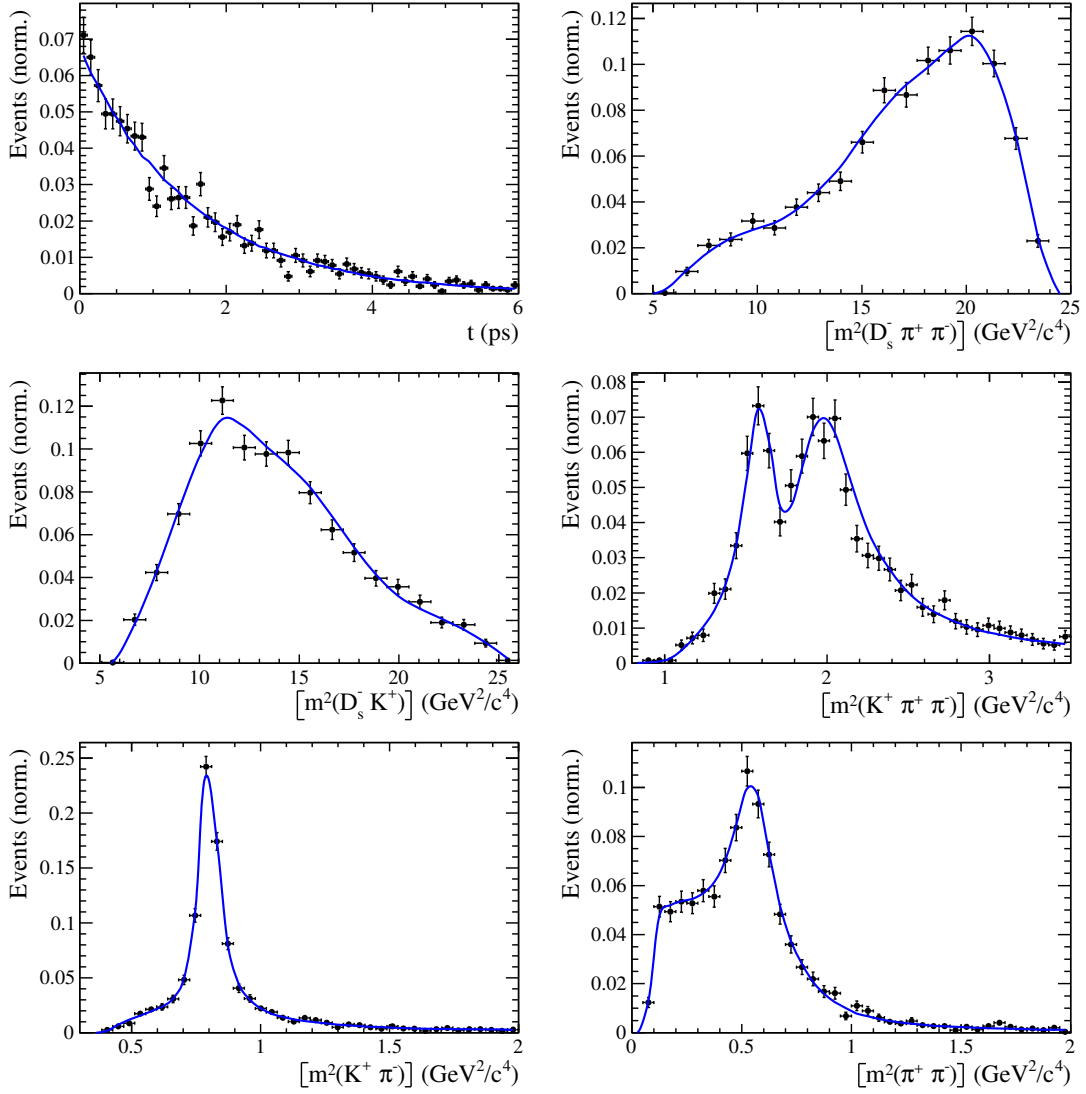
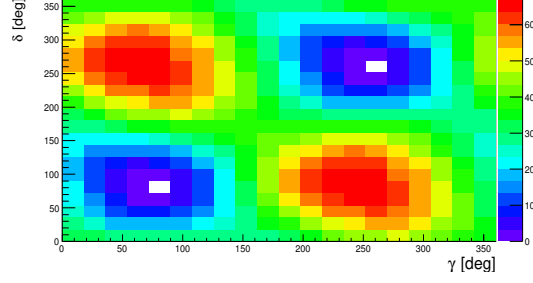


Figure 2.2: Example toy fit



Generated values:

$$\gamma = 70^\circ, \delta = 100^\circ$$

Fit result:

$$\gamma = 74 \pm 15^\circ, \delta = 84 \pm 15^\circ$$

$$(\gamma = 254 \pm 15^\circ, \delta = 264 \pm 15^\circ)$$

Figure 2.3: Likelihood scan

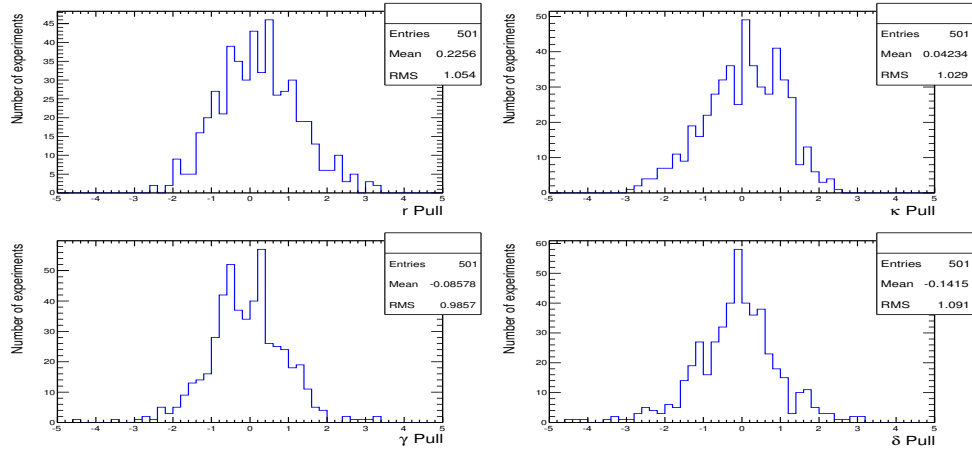


Figure 2.4: Pulls

Table 2.2

	Generated	Full PDF	Phasespace integrated
$r$	0.4	$0.38 \pm 0.06$	unstable
$\kappa$	0.2	$0.23 \pm 0.13$	0.2 (fixed)
$\delta$	100	$99 \pm 22$	unstable
$\gamma$	70	$70 \pm 17$	unstable
	Generated	Full PDF	Phasespace integrated
$r$	0.4	$0.44 \pm 0.07$	$0.43 \pm 0.11$
$\kappa$	0.4	$0.41 \pm 0.14$	0.4 (fixed)
$\delta$	100	$101 \pm 19$	$95 \pm 41$
$\gamma$	70	$69 \pm 16$	$66 \pm 40$
	Generated	Full PDF	Phasespace integrated
$r$	0.4	$0.41 \pm 0.08$	$0.39 \pm 0.11$
$\kappa$	0.6	$0.60 \pm 0.13$	0.6 (fixed)
$\delta$	100	$98 \pm 17$	$92 \pm 25$
$\gamma$	70	$68 \pm 17$	$65 \pm 28$
	Generated	Full PDF	Phasespace integrated
$r$	0.4	$0.42 \pm 0.09$	$0.39 \pm 0.09$
$\kappa$	1.0	$0.96 \pm 0.03$	1.0 (fixed)
$\delta$	100	$100 \pm 17$	$100 \pm 17$
$\gamma$	70	$66 \pm 17$	$67 \pm 17$

### 3 Selection

For the presented analysis, we reconstruct the  $B_s^0 \rightarrow D_s K \pi \pi$  decay through three different final states of the  $D_s$  meson,  $D_s \rightarrow K K \pi$ ,  $D_s \rightarrow K \pi \pi$  and  $D_s \rightarrow \pi \pi \pi$ . Of those three final states  $D_s \rightarrow K K \pi$  is the most prominent one, while  $\mathcal{BR}(D_s \rightarrow \pi \pi \pi) \approx 0.2 \cdot \mathcal{BR}(D_s \rightarrow K K \pi)$  and  $\mathcal{BR}(D_s \rightarrow K \pi \pi) \approx 0.1 \cdot \mathcal{BR}(D_s \rightarrow K K \pi)$  holds for the other two.

A two-fold approach is used to isolate the  $B_s^0 \rightarrow D_s K \pi \pi$  candidates from data passing the stripping line. First, further one-dimensional cuts are applied to reduce the level of combinatorial background and to veto some specific physical background. This stage is specific to the respective final state in which the  $D_s$  meson is reconstructed, since different physical backgrounds, depending on the respective final state, have to be taken into account. After that, a multivariate classifier is trained which combines the information of several input variables, including their correlation, into one powerful discriminator between signal and combinatorial background. For this stage, all possible  $D_s$  final states are treated equally.

#### 3.1 Cut-based selection

In order to minimize the contribution of combinatorial background to our samples, we apply the following cuts to the b hadron:

- $\text{DIRA} > 0.99994$
- $\min \text{IP } \chi^2 < 20$  to any PV,
- $\text{FD } \chi^2 > 100$  to any PV,
- $\text{Vertex } \chi^2/\text{nDoF} < 8$ ,
- $(Z_{D_s} - Z_{B_s^0}) > 0$ , where  $Z_M$  is the z-component of the position  $\vec{x}$  of the decay vertex for the  $B_s^0/D_s$  meson.

Additionally, we veto various physical backgrounds, which have either the same final state as our signal decay, or can contribute via a single misidentification of  $K \rightarrow \pi$  or  $K \rightarrow p$ . In the following, the vetoes are ordered by the reconstructed  $D_s$  final state they apply to:

##### 1. All:

- (a)  $B_s^0 \rightarrow D_s^+ D_s^- : |M(K \pi \pi) - m_{D_s}| > 20 \text{ MeV}/c^2$ .
- (b)  $B_s^0 \rightarrow D_s^- K^+ K^- \pi^+ : \text{possible with single missID of } K^- \rightarrow \pi^-$ , rejected by requiring  $\pi^-$  to fulfill  $\text{DLL}_{K\pi} < 5$ .

##### 2. $D_s \rightarrow K K \pi$

- (a)  $B^0 \rightarrow D^+(\rightarrow K^+ \pi^- \pi^+) K \pi \pi : \text{possible with single missID of } \pi^+ \rightarrow K^+$ , vetoed by changing particle hypothesis and recompute  $|M(K^+ \pi^- \pi^+) - m_{Dp}| > 30 \text{ MeV}/c^2$ , or the  $K^+$  has to fulfill  $\text{DLL}_{K\pi} > 10$ .

(b)  $\Lambda_b^0 \rightarrow \Lambda_c^+(\rightarrow pK^-\pi^+)K\pi\pi$  : possible with single missID of  $p \rightarrow K^+$ , vetoed by changing particle hypothesis and recompute  $M(pK^-\pi^+) - m_{\Lambda_c^+} > 30 \text{ MeV}/c^2$ , or the  $K^+$  has to fulfill  $(\text{DLL}_{K\pi} - \text{DLL}_{p\pi}) > 5$ .

(c)  $D^0 \rightarrow KK$  :  $D^0$  combined with a random  $\pi$  can fake a  $D_s \rightarrow KK\pi$  decay and be a background to our signal, vetoed by requiring  $M(KK) < 1840 \text{ MeV}/c^2$ .

### 3. $D_s \rightarrow K\pi\pi$

(a)  $D^0 \rightarrow \pi^+K^-$  :  $D^0$  combined with a random  $\pi^-$  can fake a  $D_s^- \rightarrow K^-\pi^+\pi^-$  decay and be a background to our signal, vetoed by requiring  $M(\pi^+K^-) < 1750 \text{ MeV}/c^2$ .

(b)  $\Lambda_b^0 \rightarrow \Lambda_c^+(\rightarrow p\pi^-\pi^+)K\pi\pi$  : possible with single missID of  $p \rightarrow K^+$ , vetoed by changing particle hypothesis and recompute  $M(p\pi^-\pi^+) - m_{\Lambda_c^+} > 30 \text{ MeV}/c^2$ , or the  $K^+$  has to fulfill  $(\text{DLL}_{K\pi} - \text{DLL}_{p\pi}) > 5$ .

### 4. $D_s \rightarrow \pi\pi\pi$

(a)  $D^0 \rightarrow \pi\pi$  : combined with a random  $\pi$  can fake a  $D_s \rightarrow \pi\pi\pi$  decay and be a background to our signal, vetoed by requiring both possible combinations to have  $M(\pi\pi) < 1700 \text{ MeV}/c^2$ .

The most prominent final state used in this analysis is  $B_s^0 \rightarrow D_s(\rightarrow KK\pi)K\pi\pi$ , where the  $D_s$  decay can either proceed via the narrow  $\phi$  resonance, the broader  $K^{*0}$  resonance, or non resonant. Depending on the decay process being resonant or not, we apply additional PID requirements on this final state:

- resonant case:

- $D_s^+ \rightarrow \phi\pi^+$ , with  $|M(K^+K^-) - m_\phi| < 20 \text{ MeV}/c^2$  : no additional requirements, since  $\phi$  is narrow and almost pure  $K^+K^-$ .

- $D_s^+ \rightarrow \bar{K}^{*0}K^+$ , with  $|M(K^-\pi^+) - m_{K^{*0}}| < 75 \text{ MeV}/c^2$  :  $\text{DLL}_{K\pi} > 0$  for kaons, since this resonance is more than ten times broader than  $\phi$ .

- non resonant case:  $\text{DLL}_{K\pi} > 5$  for kaons, since the non resonant category has significant charmless contributions.

For the other two final states, we apply global PID requirements:

- $D_s \rightarrow K\pi\pi$

- $\text{DLL}_{K\pi} > 10$  for kaons, since we expect significantly higher charmless background contribution in this channel.

- $\text{DLL}_{K\pi} < 5$  for pions.

- $D_s \rightarrow \pi\pi\pi$

- $\text{DLL}_{K\pi} < 10$  for all pions.

- $\text{DLL}_{p\pi} < 10$  for all pions.

### 3.2 Multivariate stage

We use TMVA [5] to train a multivariate discriminator, which is used to further improve the signal to background ratio. The 17 variables used for the training are:

- $\max(\text{ghostProb})$  over all tracks
- $\text{cone}(p_T)$  asymmetry of every track, which is defined to be the difference between the  $p_T$  of the  $\pi/K$  and the sum of all other  $p_T$  in a cone of radius  $r = \sqrt{(\Delta\Phi)^2 + (\Delta\eta)^2} < 1$  rad around the signal  $\pi/K$  track.
- $\min(\text{IP}\chi^2)$  over the  $X_s$  daughters
- $\max(\text{DOCA})$  over all pairs of  $X_s$  daughters
- $\min(\text{IP}\chi^2)$  over the  $D_s$  daughters
- $D_s$  and  $B_s^0$  DIRA
- $D_s$  FD significance
- $\max(\cos(D_s h_i))$ , where  $\cos(D_s h_i)$  is the cosine of the angle between the  $D_s$  and another track  $i$  in the plane transverse to the beam
- $B_s^0$   $\text{IP}\chi^2$ ,  $\text{FD}\chi^2$  and Vertex  $\chi^2$

Various classifiers were investigated in order to select the best performing discriminator. Consequently, a boosted decision tree with gradient boost (BDTG) is chosen as nominal classifier. We use truth-matched MC as signal input. Simulated signal candidates are required to pass the same trigger, stripping and preselection requirements, that were used to select the data samples. For the background we use events from the high mass sideband ( $m_{B_s^0 \text{candidate}} > 5600 \text{ MeV}/c^2$ ) of our data samples. As shown in Fig. 3.1, this mass region is sufficiently far away from signal structures and is expected to be dominantly composed of combinatorial background.

The distributions of the input variables for signal and background are shown in Fig. 3.2.

The relative importance of the input variables for the BDTG training is summarized in Table 4.1.

The BDTG output distribution for test and training samples is shown in Fig 3.3. No sign of overtraining is observed.

We determine the optimal cut value by maximizing the figure of merit  $S/\sqrt{S+B}$  where  $S$  is the signal yield and  $B$  the background yield in the signal region, defined to be within  $\pm 50 \text{ MeV}/c^2$  of the nominal  $B_s^0$  mass. To avoid a bias in the determination of the branching fraction, we determine  $S$  and  $B$  using our normalization channel. All trigger, stripping and additional selection criteria described in this and the previous chapter are applied to the  $B_s^0 \rightarrow D_s \pi \pi \pi$  data samples. After that, we perform a simplified version of the fit to the invariant mass distribution of  $B_s^0 \rightarrow D_s \pi \pi \pi$  candidates described in Sec. ???. Here, a Gaussian function to model the signal and an exponential function to model combinatorial background is used. From this fit we estimate the number of signal events

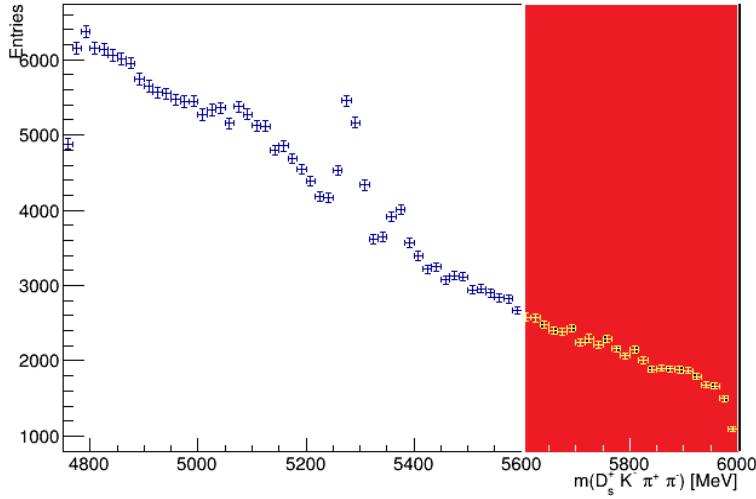


Figure 3.1: Invariant mass distribution of preselected  $B_s^0 \rightarrow D_s K \pi \pi$  candidates. The red coloured region with  $m_{B_s^0 \text{ candidate}} > 5600 \text{ MeV}/c^2$  is used as background input for the boosted decision tree.

Variable	relative importance [%]
pi_minus_ptasy_1.00	7.32
log_Ds_FDCHI2_ORIVX	7.23
K_plus_ptasy_1.00	7.17
log_Ds_DIRA	6.96
Bs_ENDVERTEX_CHI2	6.82
max_ghostProb	6.76
pi_plus_ptasy_1.00	6.57
log_DsDaughters_min_IPCHI2	6.21
log_Bs_DIRA	6.15
K_plus_fromDs_ptasy_1.00	6.10
log_XsDaughters_min_IPCHI2	5.87
K_minus_fromDs_ptasy_1.00	5.62
cos(Ds h)	5.58
log_Bs_IPCHI2_OWNPV	5.08
log_Bs_FDCHI2_OWNPV	4.04
Xs_max_DOCA	3.98
pi_minus_fromDs_ptasy_1.00	2.59

Table 3.1: Summary of the relative importance of each variable in the training of the BDTG.

189 in our normalization channel. Multiplying that number with the PDG branching fraction  
190 of  $\frac{\mathcal{B}(B_s^0 \rightarrow D_s K \pi \pi)}{\mathcal{B}(B_s^0 \rightarrow D_s \pi \pi \pi)}$  and the ratio of efficiencies discussed in Sec. ?? allows us to estimate the  
191 expected number of  $B_s^0 \rightarrow D_s K \pi \pi$  signal decays. The number of background events can  
192 then be computed as

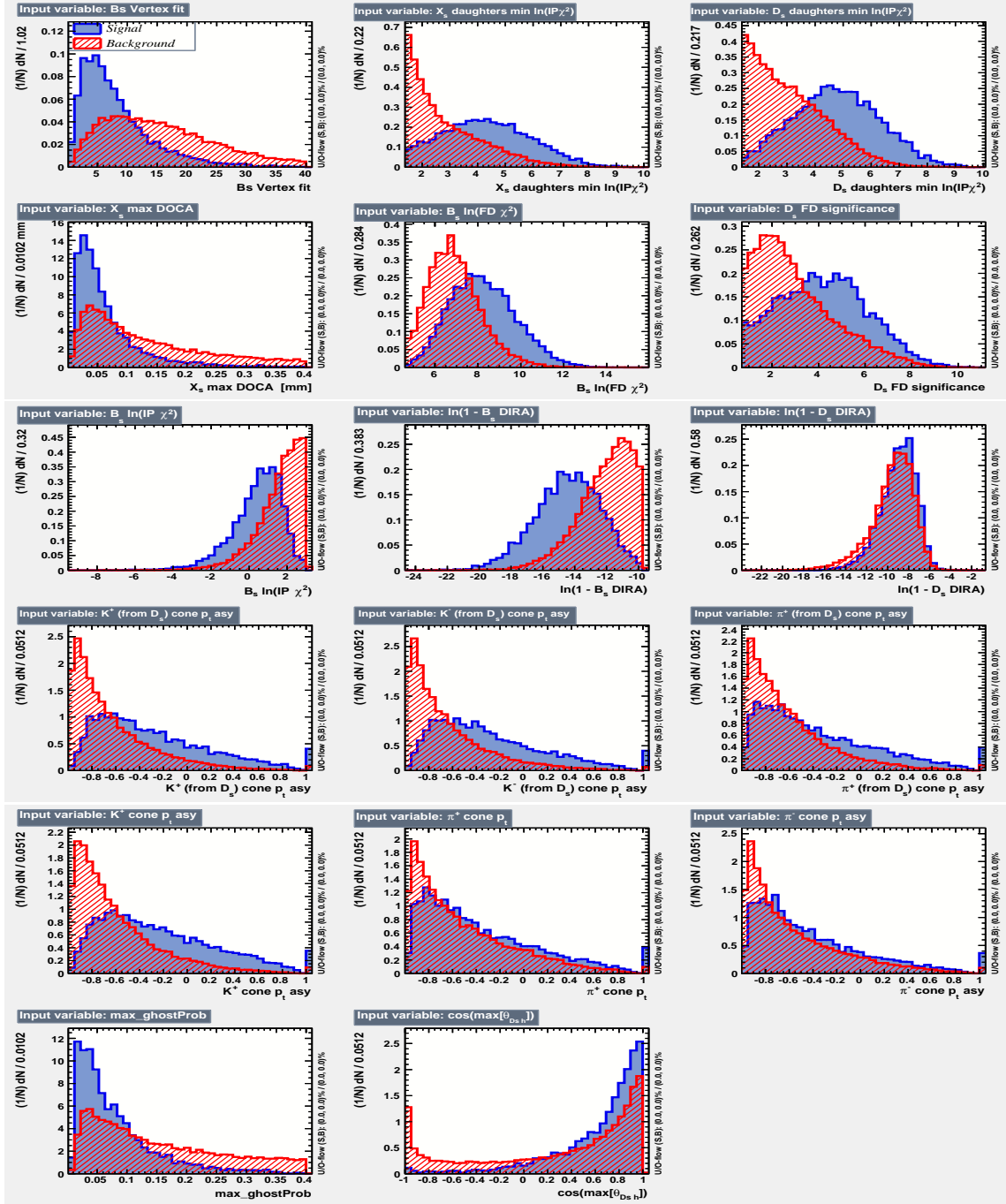


Figure 3.2: Distributions of the input variables used in the BDTG training. The background is shown as red hatched, while the signal is depicted solid blue.

$$N_{bkg} = N_{all} - N_{sig}|_{m_{B_s^0} \pm 50 \text{ MeV}/c^2}. \quad (3.1)$$

The efficiency curves as a function of the cut value are shown in Fig. 3.4. The optimal cut value is found to be  $\text{BDTG} > 0.7012$ . At this working point the signal efficiency is estimated to be 72.47 %, while the background rejection in the signal region is 97.38 %.



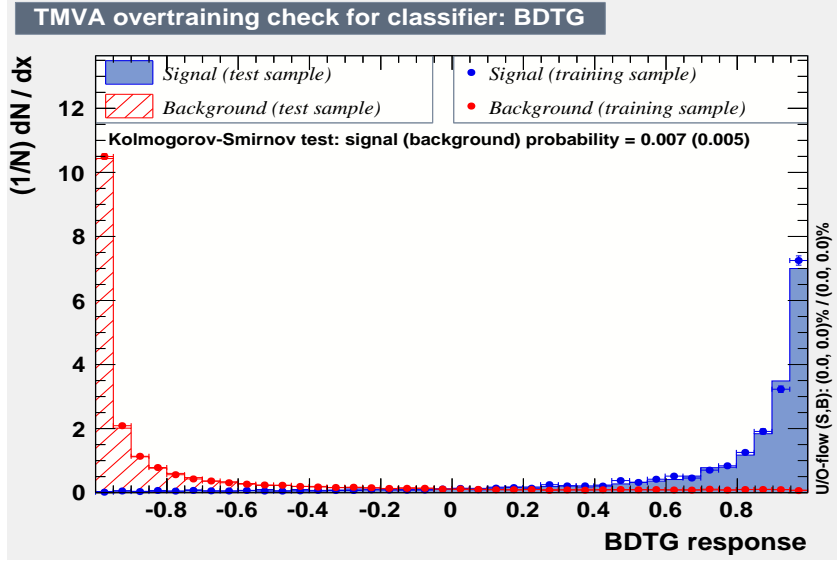


Figure 3.3: BDTG output classifier distribution for (blue) signal and (red) background. The response of an independent test sample (dots) is overlaid.

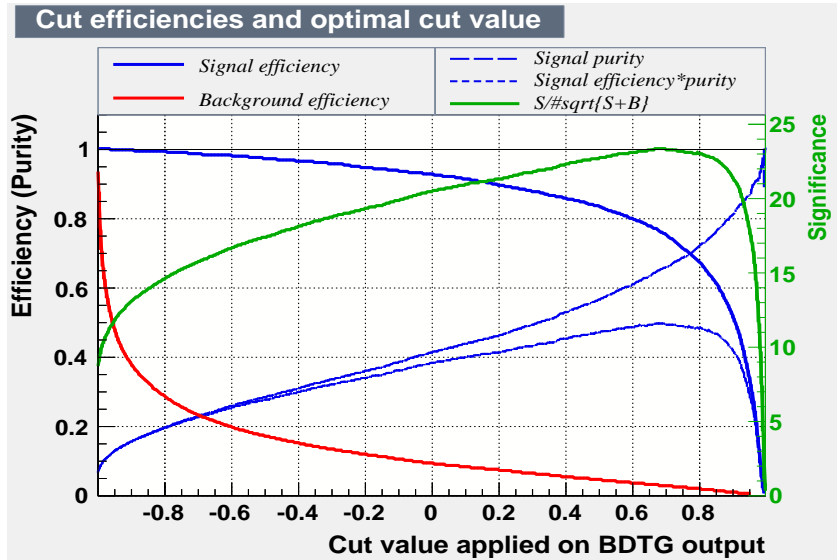


Figure 3.4: Efficiency and purity curves for (blue) signal, (red) background and the (green) FoM curve, as a function of the chosen cut value.

## 4 Decay-time Acceptance

The decay-time distribution of the  $B_s^0$  mesons is sculpted due to the geometry of the LHCb detector and the applied selection cuts, which are described in Section 3. In particular, any requirement on the flight distance (FD), the impact parameter (IP) or the direction angle (DIRA) of the  $B_s^0$  mesons, as well as the direct cut on the lifetime, will lead to a decay-time dependent efficiency  $a(t)$ . This efficiency will distort the theoretically expected, time-dependent decay rate

$$\frac{\Gamma(t)^{observed}}{dt} = \frac{\Gamma(t)^{theory}}{dt} \cdot a(t), \quad (4.1)$$

and has to be modelled correctly, in order to describe the observed decay rate. We use our control channel for this measurement, because for  $B_s^0 \rightarrow D_s K \pi \pi$  decays the decay-time acceptance is correlated with the CP-observables which we aim to measure. Therefore, floating the CP-observables and the acceptance shape at the same time is not possible. Hence, a fit to the decay-time distribution of  $B_s^0 \rightarrow D_s \pi \pi \pi$  candidates is performed and the obtained acceptance shape is corrected by the difference in shape found for the  $B_s^0 \rightarrow D_s K \pi \pi$  and  $B_s^0 \rightarrow D_s \pi \pi \pi$  MC.

A PDF of the form

$$\mathcal{P}(t', \vec{\lambda}) = \left[ (e^{\Gamma_s t} \cdot \cosh(\frac{\Delta \Gamma_s t}{2}) \times \mathcal{R}(t - t')) \cdot \epsilon(t', \vec{\lambda}) \right], \quad (4.2)$$

is fit to the decay time distribution of  $B_s^0 \rightarrow D_s \pi \pi \pi$  candidates in data. Since the fit is performed untagged, the PDF shown in Eq. 4.2 contains no terms proportional to  $\Delta m_s$ . The values for  $\Gamma_s$  and  $\Delta \Gamma_s$  are fixed to the latest HFAG results [6]. The decay-time acceptance  $\epsilon(t', \vec{\lambda})$  is modelled using the sum of cubic polynomials  $v_i(t)$ , so called Splines [7]. The polynomials are parametrised by so-called knots which determine their boundaries. Knots can be set across the fitted distribution to account for local changes in the acceptance shape. Using more knots is equivalent to using more base splines which are defined on a smaller sub-range. In total,  $n + 2$  base splines  $v_i(t)$  are needed to describe an acceptance shape which is parametrised using  $n$  knots.

For fits shown in the following, the knots have been placed at  $t = [0.5, 1.0, 1.5, 2.0, 3.0, 9.5]ps$ . To accomodate these 6 knot positions, 8 basic splines  $v_i$ ,  $i = [1, \dots, 8]$  are used. Since a rapid change of the decay time acceptance at low decay times due to the turn-on effect generated by the lifetime and other selection cuts is expected, more knots are placed in that regime. At higher decay times we expect linear behaviour, with a possible small effect due to the VELO reconstruction. Therefore fewer knots are used. Furthermore,  $v_7$  is fixed to 1 in order to normalize the overall acceptance function. To stabilise the last spline,  $v_8$  is fixed by a linear extrapolation from the two previous splines:

$$v_N = v_{N-1} + \frac{v_{N-2} - v_{N-1}}{t_{N-2} - t_{N-1}} \cdot (t_N - t_{N-1}). \quad (4.3)$$

Here,  $N = 8$  and  $t_{N-1}$  corresponds to the knot position associated with  $v_{N-1}$ . The nominal fit to  $B_s^0 \rightarrow D_s \pi \pi \pi$  data using this configuration is shown in Figure 4.1. Note that the normalization of the splines in the following figures is not in scale.

The fits to  $B_s^0 \rightarrow D_s \pi \pi \pi$  and  $B_s^0 \rightarrow D_s K \pi \pi$  simulation are shown in Figure 4.2.

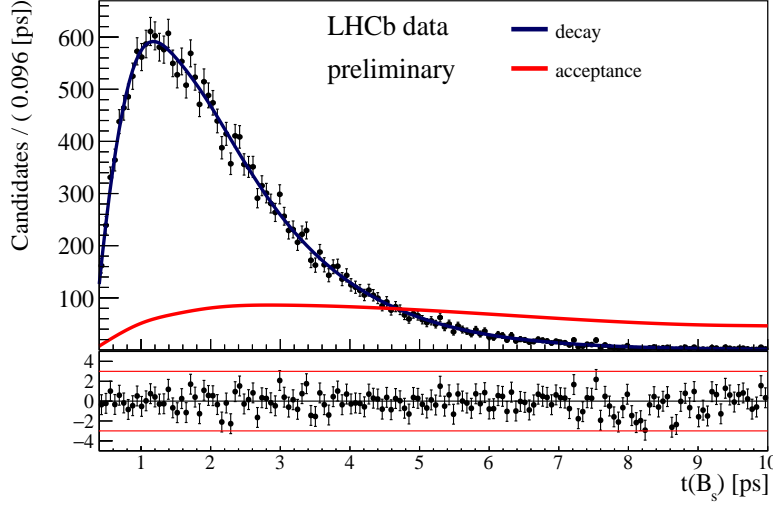


Figure 4.1: Decay-time distribution of  $B_s^0 \rightarrow D_s \pi \pi \pi$  candidates for the Run 1 data sample. The fit described in the text is overlaid. The red line shows the spline function describing the acceptance and the blue line depicts the total fit function.

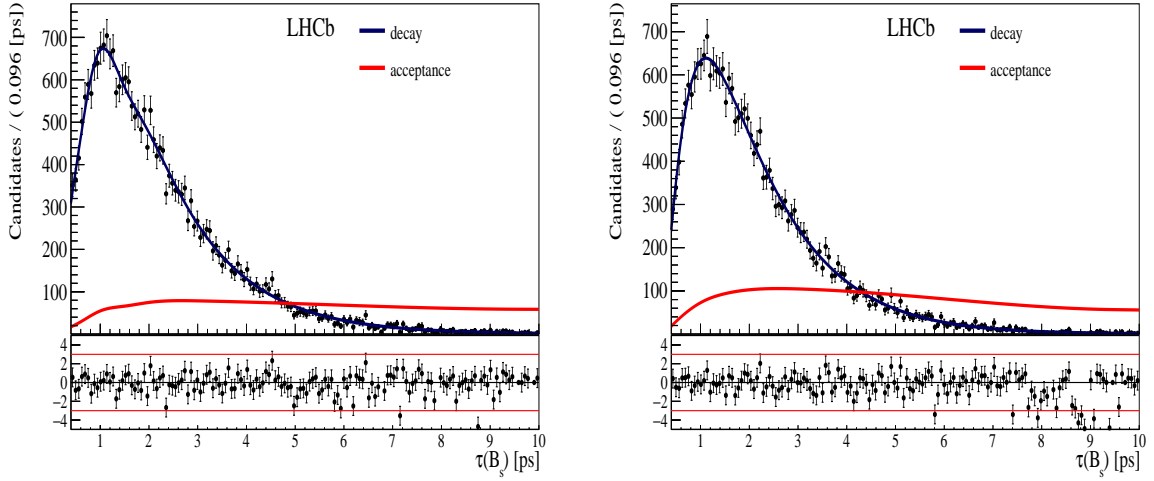


Figure 4.2: Decay-time distribution of (left)  $B_s^0 \rightarrow D_s \pi \pi \pi$  and (right)  $B_s^0 \rightarrow D_s K \pi \pi$  candidates in MC using truth information. The fit described in the text is overlaid. The red line shows the spline function describing the acceptance and the blue line depicts the total fit function.

233 The fit parameters obtained from the described fits to data and simulation are  
 234 summarised in Tab. xXx.

Parameter	Fit to $B_s^0 \rightarrow D_s \pi \pi \pi$ data	Fit to $B_s^0 \rightarrow D_s \pi \pi \pi$ MC	Fit to $B_s^0 \rightarrow D_s K \pi \pi$ MC
$v_1$			
$v_2$			
$v_3$			
$v_4$			
$v_5$			
$v_6$			
$v_7$	fixed	fixed	fixed

Table 4.1: Summary of the obtained parameters from the acceptance fits described above.

## 5 Decay-time Resoution

The observed oscillation of B mesons is prone to dilution, if the detector resolution is of similar magnitude as the oscillation period. In the  $B_s^0$  system, considering that the measured oscillation frequency of the  $B_s^0$  [8] and the average LHCb detector resolution [9] are both  $\mathcal{O}(50 \text{ fs}^{-1})$ , this is the case. Therefore, it is crucial to correctly describe the decay time resolution in order to avoid a bias on the measurement of time dependent CP parameters.

In the presented analysis, we assume a gaussian resolution function with different widths for each event. This gives rise to a per-event decay time error  $\sigma_t$ , which is computed separately for every event along with the proper time  $t$ , by the decay time fitter. Furthermore, the per-event decay time error  $\sigma_t$  is usually underestimated by the decay time fitter, making it necessary to derive a scaling function, which matches the per-event error to the actually measured decay time resolution. In the following, we investigate the Run1 and Run2 MC samples to find the proper decay time resolution in bins of the per-event decay time erros and derive a scaling function from that.

### 5.1 Formalism

Description here ...

### 5.2 Results

Summary of results and MC/Data correction from  $D_s K$  here ...

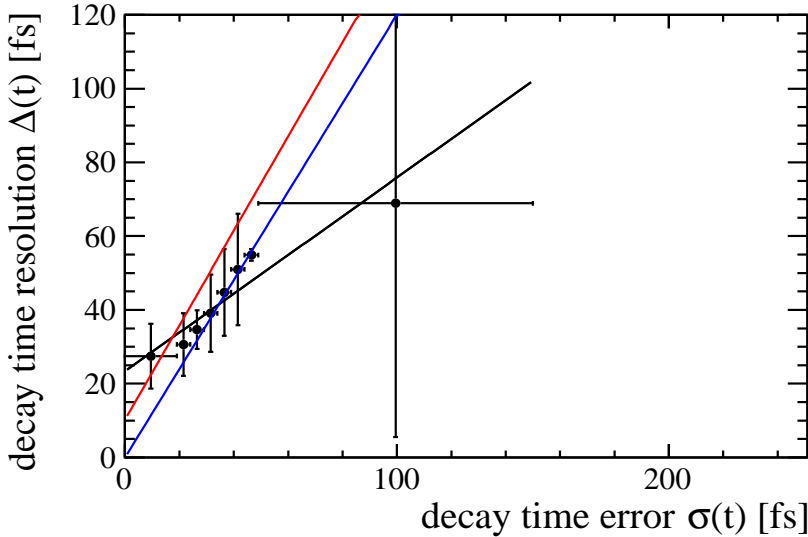


Figure 5.1: Decay-time resolution of  $B_s^0 \rightarrow D_s K \pi \pi$  candidates from MC. The fit described in the text is overlaid.

$\sigma_t$ Bin [fs]	$\sigma_1$ [fs]	$\sigma_2$ [fs]	$f_1$	D	$\sigma_{eff}$ [fs]
0to19	$22.57 \pm 0.96$	$45.57 \pm 4.061$	$0.827 \pm 0.057$	$0.89 \pm 0.067$	$27.46 \pm 8.82$
19to24	$24.64 \pm 1.03$	$46.65 \pm 3.109$	$0.768 \pm 0.061$	$0.86 \pm 0.070$	$30.64 \pm 8.48$
24to29	$30.96 \pm 0.90$	$58.76 \pm 5.684$	$0.884 \pm 0.045$	$0.83 \pm 0.05$	$34.66 \pm 5.28$
29to34	$35.28 \pm 1.54$	$57 \pm 6.698$	$0.839 \pm 0.098$	$0.79 \pm 0.10$	$39.09 \pm 10.47$
34to39	$37.05 \pm 2.36$	$61.98 \pm 5.769$	$0.707 \pm 0.12$	$0.73 \pm 0.12$	$44.76 \pm 11.78$
39to44	$68.38 \pm 8.33$	$42.15 \pm 3.583$	$0.331 \pm 0.18$	$0.66 \pm 0.16$	$50.98 \pm 15.11$
44to49	$199.9 \pm 100.1$	$53.72 \pm 1.419$	$0.020 \pm 0.014$	$0.62 \pm 0.02$	$54.89 \pm 1.60$
49to150	$68.75 \pm 165.3$	$68.92 \pm 4.603$	$0.001 \pm 0.97$	$0.47 \pm 0.65$	$68.92 \pm 63.42$

Table 5.1: Summary of the obtained parameters from the resolution fits described above.

## References

- [1] R. Fleischer, *New strategies to obtain insights into CP violation through  $B(s) \rightarrow D(s)^\pm K^\mp$ ,  $D(s)^* K^\pm$ ,  $D(s)^* K^\mp$ , ... and  $B(d) \rightarrow D^\pm \pi^\mp$ ,  $D^* K^\pm$ ,  $D^* K^\mp$ , ... decays*, Nucl. Phys. **B671** (2003) 459, [arXiv:hep-ph/0304027](#).
- [2] K. De Bruyn *et al.*, *Exploring  $B_s \rightarrow D_s^{(*)\pm} K^\mp$  Decays in the Presence of a Sizable Width Difference  $\Delta\Gamma_s$* , Nucl. Phys. **B868** (2013) 351, [arXiv:1208.6463](#).
- [3] S. Blusk, *First observations and measurements of the branching fractions for the decays  $\bar{B}_s^0 \rightarrow D_s^+ K^- \pi^+ \pi^-$  and  $\bar{B}^0 \rightarrow D_s^+ K^- \pi^+ \pi^-$* , .
- [4] LHCb, S. Blusk, *Measurement of the CP observables in  $\bar{B}_s^0 \rightarrow D_s^+ K^-$  and first observation of  $\bar{B}_{(s)}^0 \rightarrow D_s^+ K^- \pi^+ \pi^-$  and  $\bar{B}_s^0 \rightarrow D_{s1}(2536)^+ \pi^-$* , 2012. [arXiv:1212.4180](#).
- [5] A. Hoecker *et al.*, *TMVA: Toolkit for Multivariate Data Analysis*, PoS **ACAT** (2007) 040, [arXiv:physics/0703039](#).
- [6] Heavy Flavor Averaging Group, Y. Amhis *et al.*, *Averages of b-hadron, c-hadron, and  $\tau$ -lepton properties as of summer 2014*, [arXiv:1412.7515](#), updated results and plots available at <http://www.slac.stanford.edu/xorg/hfag/>.
- [7] T. M. Karbach, G. Raven, and M. Schiller, *Decay time integrals in neutral meson mixing and their efficient evaluation*, [arXiv:1407.0748](#).
- [8] Particle Data Group, K. A. Olive *et al.*, *Review of particle physics*, Chin. Phys. **C38** (2014) 090001, and 2015 update.
- [9] LHCb collaboration, R. Aaij *et al.*, *LHCb detector performance*, Int. J. Mod. Phys. **A30** (2015) 1530022, [arXiv:1412.6352](#).